Mass Transport Investigated with the Electrochemical and Electrogravimetric Impedance Techniques. 3. Complex Charge Transport in PPy/PSS Films

Haesik Yang and Juhyoun Kwak*

Department of Chemistry, Korea Advanced Institute of Science and Technology, Taejon 305-701, Korea

Received: August 28, 1997; In Final Form: November 24, 1997

For the first time, the complex charge transport mechanism for polypyrrole/poly(polystyrenesulfonate) (PPy/PSS) films in aqueous electrolyte solutions has been revealed by employing the cyclic/step electrochemical quartz crystal microbalance (EQCM) technique and the electrochemical/electrogravimetric impedance technique. Especially from the impedance experiments, the relative diffusion coefficient of charge transport has been obtained, and also the ion transport behavior in the slow charge transport process has been revealed. In PPy/PSS films, anion transport is considerable in the slow charge transport process, while cation transport is dominant in the fast charge transport process. It is shown that the presence of the slow charge transport processes is due to a slow electron transport process, not a slow ion transport process.

Introduction

The redox reaction of a conducting polymer film[1] is accompanied by the movement of ions in order to maintain electroneutrality inside the film.[2] Its electrochemical application is in need of selective or fast ion transport. There have been many studies to increase the selectivity of ion transport and the diffusion coefficient of an ion in the polymer film.[3] Thus, it is very important to obtain effectively the relative contributions of a cation and an anion to ion transport and their diffusion coefficients.

In many conducting polymer/electrolyte systems, the ion transport behavior is neither cation-selective nor anion-selective, and thus it is complex.[4] To study the ion transport mechanism, the electrochemical quartz crystal microbalance (EQCM) technique[5] has been used widely. Information on the dominant moving ion can be easily obtained from this technique. However, it is difficult to reveal the exact contributions of a cation and an anion because ion transport is accompanied by solvent transport.[6] Moreover, the relative contributions of a cation and an anion change as the scan rate varies in the cyclic EQCM experiment, because the diffusion coefficient of a cation in a film is different from that of an anion.[4a] Therefore, there is a limit to obtaining the relative contribution of an ion by use of the EQCM technique only. The contribution of an ion should be obtained with its diffusion coefficient.

The diffusion coefficient of an ion in a film can be obtained by using the electrochemical impedance technique.[2b,7] The technique enables us to study even the slow diffusion process that cannot be observed easily with other techniques.[8] Two semicircles have been observed in the electrochemical capacitance plots for polypyrrole (PPy) films,[8,9] polyaniline films,[10] and ruthenium oxide films.[11] From the presence of two semicircles in PPy films, it has been proposed that the redox reaction of PPy films is divided into the fast faradaic process and the slow faradaic process.[8] For the general discussion, the fast and slow faradaic processes are referred to as the fast and slow charge transport processes here. Because there is no chemical information on the moving ion in the electrochemical impedance data, it is not known whether ion transport in each charge transport process, especially the slow charge transport process, is cation-dominant or anion-dominant. The electrogravimetric impedance technique is another powerful technique[12] for the study of the ion transport mechanism. When the technique is combined with the electrochemical impedance technique, the diffusion coefficients and contributions of a cation and an anion can be obtained simultaneously as a function of the redox state of a film.[13]

Although much of the work has been focused on the ion transport mechanism in PPy films, the current state is still far from its full understanding. To understand the complex ion transport mechanism, the studies on the number of accompanying waters per ion must be preceded; then, the contribution of an ion to ion transport and its diffusion coefficient can be investigated. Recently, we have obtained important information on the number of accompanying waters per ion during the redox reaction of PPy films and poly(*N*-methylpyrrole) films.[14]

In this paper, the complex charge transport mechanism for polypyrrole/poly(polystyrenesulfonate) (PPy/PSS) films,[6b] where cation transport is dominant in the fast charge transport process, has been investigated from the cyclic/step EQCM experiments and the electrochemical/electrogravimetric impedance experiments. First, the relation between the electrogravimetric capacitance plot and the ion transport behavior has been investigated in the case where two kinds of ion take part in ion transport. Second, the gravimetric and electrical responses have been compared in terms of the film thickness. Third, the contributions of a cation and an anion to ion transport and the relative diffusion coefficient of charge transport have been obtained. Finally, the slow charge transport process is discussed in connection with both electron and ion transport.

Experimental Section

Chemicals. Pyrrole, sodium poly(styrenesulfonate) (NaPSS), Cs_2SO_4, and $CsNO_3$ were purchased from Aldrich and used as received. Double-distilled water was used for the preparation of all solutions.

* To whom correspondence should be addressed.

S1089-5647(97)02820-4 CCC: $15.00
Published on Web 02/18/1998

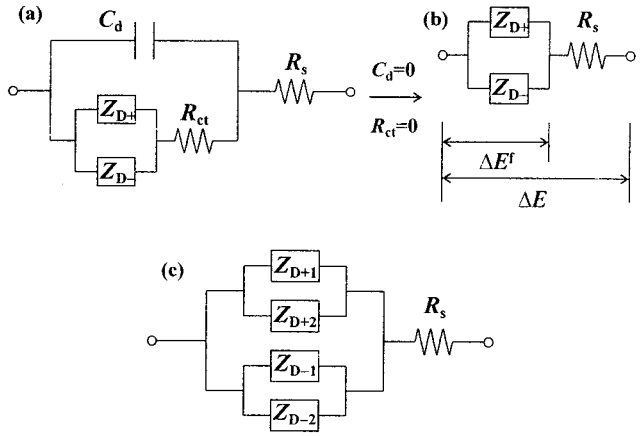

Figure 1. (a) Modified Randle's equivalent circuit in the case of cation and anion transport: R_s, the solution resistance; R_{ct}, the charge-transfer resistance; C_d, the double-layer capacitance; $\mathbf{Z_{D+}}$, the diffusion impedance of a cation in a film; $\mathbf{Z_{D-}}$, the diffusion impedance of an anion. (b) Equivalent circuit where R_{ct} and C_d are negligible. (c) Equivalent circuit where both cation and anion transport occur in the slow and fast charge transport processes.

Electrochemistry and Film Preparation. An electrochemical cell and electrodes used in this study were the same as those reported previously.[14a] All potentials are reported relative to Ag/AgCl. PPy/PSS films were grown potentiostatically at 0.60 V in a solution of 0.1 M pyrrole and 0.1 M NaPSS. The film thickness is estimated by assuming that 300 mC/cm^2 corresponds approximately to 1 μm in consideration of the reported value.[8]

Instrumentation and Data Treatment. The experimental apparatus and the data treatment were also described previously.[14a] The separated electrochemical capacitance data were fitted by using the complex nonlinear least-squares (CNLS) fitting program. The CNLS program used in this work is the LEVM program (Scribner, VA).[7b]

Results and Discussion

Electrogravimetric Capacitance Plot in the Case of Two Kinds of Ion Transport. When both cation and anion take part in ion transport, the relation between mass change (ΔM) and charge change (ΔQ) is simple as follows[14a]

$$\Delta M = -\frac{W_+'}{z_+F}\Delta Q_+ - \frac{W_-'}{z_-F}\Delta Q_- \qquad (1)$$

where

$$W' = W + YW_s \qquad (2)$$

In above equations, the subscripts + and − represent cation and anion, respectively, W' is the molar mass of an ion and accompanying solvents, z is the electric charge of an ion, F is the faradaic constant, W is the molar mass of an ion, Y is the number of accompanying solvents per ion, and W_s is the molar mass of a solvent.

The equivalent circuit for dual ion transport in a polymer film (Figure 1a) contains the finite diffusion impedance of a cation ($\mathbf{Z_{D+}}$) and the finite diffusion impedance of an anion ($\mathbf{Z_{D-}}$) that are connected parallel. The mathematical form of the impedance $\mathbf{Z_D}$ is given by[8,15]

$$\mathbf{Z_D} = R_D \frac{\coth\sqrt{j\omega R_D C_D}}{\sqrt{j\omega R_D C_D}} \qquad (3)$$

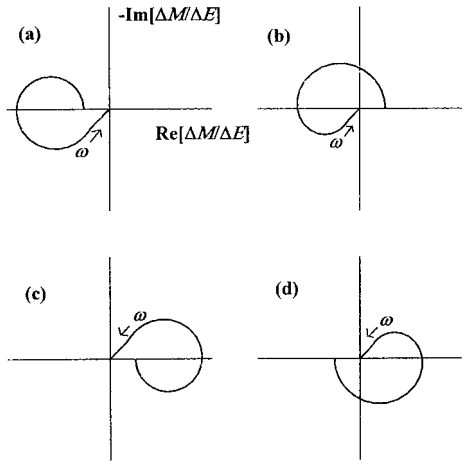

Figure 2. Electrogravimetric capacitance ($\mathbf{\Delta M}/\mathbf{\Delta E}$) plots in terms of R_DC_D and C_D of both $\mathbf{Z_{D+}}$ and $\mathbf{Z_{D-}}$: (a) $R_{D+}C_{D+} < R_{D-}C_{D-}$ and $-(W'/z_+F)C_{D+} > -(W'/z_-F)C_{D-}$; (b) $R_{D+}C_{D+} < R_{D-}C_{D-}$ and $-(W'/z_+F)C_{D+} < -(W'/z_-F)C_{D-}$; (c) $R_{D+}C_{D+} > R_{D-}C_{D-}$ and $-(W'/z_+F)C_{D+} < -(W'/z_-F)C_{D-}$; and (d) $R_{D+}C_{D+} > R_{D-}C_{D-}$ and $-(W'/z_+F)C_{D+} > -(W'/z_-F)C_{D-}$.

where R_D is the ionic resistance in a film, C_D is the redox capacitance in a film, j is $\sqrt{-1}$, and ω is an angular frequency.

Figure 2 shows the electrogravimetric capacitance ($\mathbf{\Delta M}/\mathbf{\Delta E}$) plots for the ($\mathbf{\Delta M}/\mathbf{\Delta E}$) data simulated by considering both $\mathbf{Z_{D+}}$ and $\mathbf{Z_{D-}}$ in terms of R_DC_D time and C_D. R_DC_D time is inversely proportional to the diffusion coefficient of an ion in a film as described later,[16] and C_D is proportional to the amount of ion transport. In the electrochemical capacitance ($\mathbf{\Delta Q}/\mathbf{\Delta E}$) plot, the size of an electrochemical semicircle depends on C_D, while the position of the ($\mathbf{\Delta Q}/\mathbf{\Delta E}$) data depends on R_DC_D time. The electrogravimetric one corresponding to R_D is $-(zF/W')R_D$, and the electrogravimetric one corresponding to C_D is $-(W'/zF)C_D$. Thus, in the ($\mathbf{\Delta M}/\mathbf{\Delta E}$) plot, the size of an electrogravimetric semicircle depends on $-(W'/zF)C_D$, while the position of the ($\mathbf{\Delta M}/\mathbf{\Delta E}$) data depends on R_DC_D time. In Figure 2a,b where the diffusion coefficient of a cation is larger than that of an anion, the influence of a cation is dominant in the high frequency region, and the influence of an anion increases as frequency decreases. This trend is reversed in Figure 2c,d where the diffusion coefficient of an anion is larger than that of a cation.

If the charge transfer resistance (R_{ct}) and the double layer capacitance (C_d) is negligible, the equivalent circuit is reduced to series connection of the diffusion impedance and the solution resistance (R_s) (Figure 1b). In this case, ΔQ is equal to ΔQ^f, and also ΔM is equal to ΔM^f. To obtain the faradaic electrochemical capacitance ($\mathbf{\Delta Q^f}/\mathbf{\Delta E^f}$) and the faradaic electrogravimetric capacitance ($\mathbf{\Delta M^f}/\mathbf{\Delta E^f}$), the effect of R_s on the capacitance data must be corrected. As shown in Figure 1b, the ratio of the faradaic potential (ΔE^f) to the applied potential (ΔE) is equal to $(\mathbf{Z} - R_s)/\mathbf{Z}$, where $\mathbf{Z}$ is ($\mathbf{\Delta E}/\mathbf{\Delta I}$). Thus, ($\mathbf{\Delta Q^f}/\mathbf{\Delta E^f}$) and ($\mathbf{\Delta M^f}/\mathbf{\Delta E^f}$) are represented as follows:

$$\left(\frac{\mathbf{\Delta Q^f}}{\mathbf{\Delta E^f}}\right) = \left(\frac{\mathbf{\Delta Q}}{\mathbf{\Delta E}}\right)\left(\frac{\mathbf{\Delta E}}{\mathbf{\Delta E^f}}\right) = \left(\frac{\mathbf{\Delta Q}}{\mathbf{\Delta E}}\right)\left(\frac{\mathbf{Z}}{\mathbf{Z} - R_s}\right) \qquad (4)$$

$$\left(\frac{\mathbf{\Delta M^f}}{\mathbf{\Delta E^f}}\right) = \left(\frac{\mathbf{\Delta M}}{\mathbf{\Delta E}}\right)\left(\frac{\mathbf{Z}}{\mathbf{Z} - R_s}\right) \qquad (5)$$

The faradaic electrochemical capacitance of a cation ($\mathbf{\Delta Q^f}_+/\mathbf{\Delta E^f}$) and the faradaic electrochemical capacitance of an anion ($\mathbf{\Delta Q^f}_-/\mathbf{\Delta E^f}$) can be obtained by the following two equations:

$$\left(\frac{\Delta Q^{f}}{\Delta E^{f}}\right)=\left(\frac{\Delta Q^{f}_{+}}{\Delta E^{f}}\right)+\left(\frac{\Delta Q^{f}_{-}}{\Delta E^{f}}\right) \quad (6)$$

$$\left(\frac{\Delta M^{f}}{\Delta E^{f}}\right)=\left(\frac{\Delta M^{f}_{+}}{\Delta E^{f}}\right)+\left(\frac{\Delta M^{f}_{-}}{\Delta E^{f}}\right)= -\frac{W_{+}'}{z_{+}F}\left(\frac{\Delta Q^{f}_{+}}{\Delta E^{f}}\right)-\frac{W_{-}'}{z_{-}F}\left(\frac{\Delta Q^{f}_{-}}{\Delta E^{f}}\right) \quad (7)$$

Gravimetric and Electrical Responses in Terms of the PPy/PSS Film Thickness. Figure 3 shows cyclic voltammograms and simultaneously acquired mass change diagrams for PPy/PSS films in Cs^+-containing solutions. To compare mass change rate ($G = dM/dt$) with current (I), G is normalized by the factor $-(zF/W')$, i.e., $G_n = -(zF/W')G$. Because the number of accompanying waters per Cs^+ (Y_{Cs^+}) is not large, G is normalized without consideration of water transport ($W' = W_{Cs^+}$). If only Cs^+ transport takes place, G_n matches exactly with I. G_n for the 1.5 μm film is similar to I in an overall potential range (Figure 3a). It indicates that Cs^+ transport is dominant during the redox reaction of PPy/PSS films. However, G_n for the 0.5-μm film is smaller than I in a wide potential range (Figure 3b), and G_n for the 0.2-μm film is much smaller than I (Figure 3c). It was shown that there is considerable cathodic current by the reduction of an aqueous electrolyte solution in the negative potential region.[14b] Thus, though G_n in Figure 3c at the potential region near a negative potential limit is small, I is considerable. Consequently, the large difference between I and G_n in the thin film is accounted for partly by the reduction of an aqueous solution. Because this influence occurs mainly near a negative potential limit, it is likely that the small G_n in a wide potential range is due to the participation of another species in addition to Cs^+. Considering the previous experimental results,[14] there is no possibility of the opposite movement of waters to Cs^+ movement. Therefore, it seems that the small G_n is due to anion transport and that the relative contribution of an anion to ion transport increases as the film thickness decreases.

Figure 4a−c shows chronoamperometric responses and simultaneously acquired mass change diagrams after the potential step from −0.35 V to −0.25 V in the same systems as those in Figure 3a−c. ΔQ is also normalized by the factor $-(W'/zF)$ without consideration of water transport ($W' = W_{Cs^+}$), i.e., $Q_n = -(W'/zF)Q$. The ratio of ΔM to ΔQ_n is shown in Figure 4d. During the initial time of chronoamperometry, all ratios increase with time because charging current is considerable. The highest value of the ratio is larger in the thicker film, because the contribution of charging current to total current is smaller in the thicker film. The ratio for the 1.5-μm film is close to unit after the initial rise. This shows that Cs^+ transport prevails if charging current is considered. It is interesting to note that $|\Delta M|$ for the 0.2 μm film decreases with time while $|\Delta Q_n|$ increases (Figure 4c). This indicates that, during the oxidation of the film, anion transport in addition to Cs^+ transport is considerable. All ratios of ΔM to ΔQ_n decrease gradually with time after the initial rise. This shows that anion transport in addition to Cs^+ transport increases with time. The ratio decreases more rapidly in the thinner film. This indicates that the relative contribution of an anion to ion transport is larger in the thinner film at the same measurement time.

Figure 5a,c,e shows electrochemical capacitance ($\Delta Q/\Delta E$) plots and simultaneously acquired electrogravimetric capacitance ($\Delta M/\Delta E$) plots at −0.3 V in the same systems as those in Figure 3a−c. The ($\Delta Q/\Delta E$) plot is normalized by the factor $-(W'/zF)$ without consideration of water transport ($W' = W_{Cs^+}$), i.e., $(\Delta Q/\Delta E)_n = -(W'/zF)(\Delta Q/\Delta E)$. The electrogravimetric semicircle for the 1.5 μm film is a little smaller than the normalized electrochemical one (Figure 5a), whereas the electrogravimetric semicircle for the 0.5-μm film is much smaller than the normalized electrochemical one (Figure 5c). Moreover, the electrogravimetric semicircle for the 0.2-μm film differs from the normalized electrochemical one in its shape as well as its size (Figure 5e). This indicates that, in the frequency range from 2.72 Hz to 0.04 Hz, Cs^+ transport is dominant during the redox reaction of the thick film whereas anion transport is considerable during the redox reaction of the thin film.

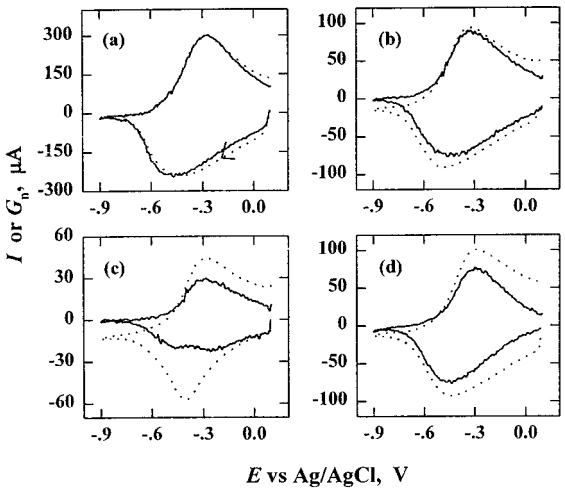

Figure 3. Cyclic voltammograms (I vs E, ···) and normalized mass change rate diagrams ($G_n = -(zF/W')G$ vs E, —) (scan rate = 10 mV/s, film thickness = (a) 1.5 μm, (b, d) 0.5 μm, and (c) 0.2 μm) for PPy/PSS films in (a, b, c) 0.5 M Cs_2SO_4 and (d) 1.0 M $CsNO_3$ ($W' = W_{Cs^+} = 132.9$).

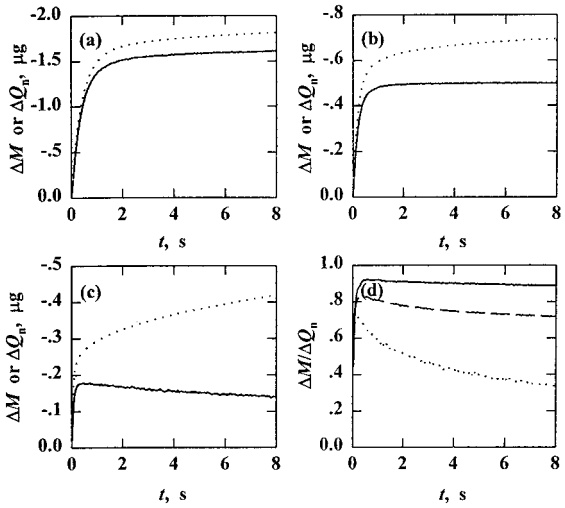

Figure 4. Chronoamperometric responses ($\Delta Q_n = -(W'/zF)\Delta Q$ vs t; ···) and simultaneously acquired mass change diagrams (ΔM vs t; —) for PPy/PSS films (film thickness = (a) 1.5 μm, (b) 0.5 μm, and (c) 0.2 μm) after the potential step from −0.35 V to −0.25 V ($W' = W_{Cs^+} = 132.9$). (d) Ratio diagram of ΔM to ΔQ_n (—, 1.5 μm, - -, 0.5 μm; ···; 0.2 μm).

Ion Transport in PPy/PSS Films. To investigate the ion transport mechanism in detail, the ($\Delta Q/\Delta E$) and ($\Delta M/\Delta E$) data for 1.0 μm thick PPy/PSS films at −0.3 V in a 0.5 M Cs_2SO_4 solution are obtained in the wide frequency range from 2.72 Hz to 4 mHz (Figure 6). Figure 6a shows a faradaic electrochemical capacitance ($\Delta Q^f/\Delta E^f$) plot, and Figure 6b shows a faradaic electrogravimetric capacitance ($\Delta M^f/\Delta E^f$) plot. The

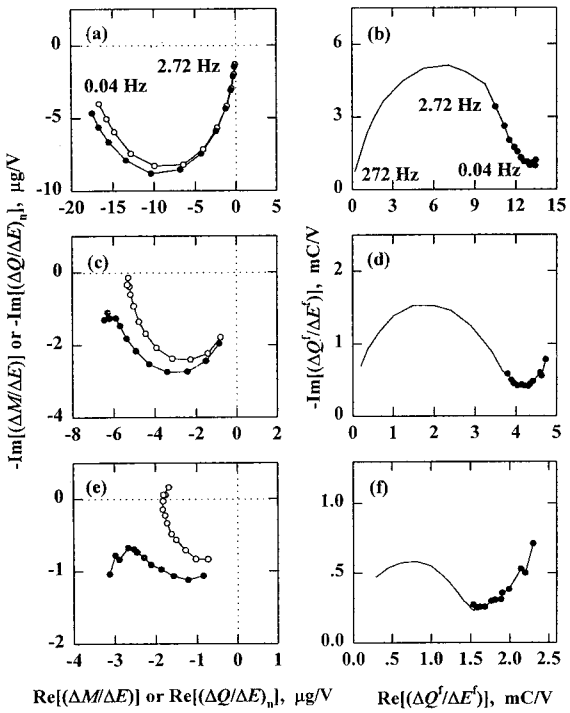

Figure 5. (a, c, e) Electrogravimetric capacitance ($(\Delta M/\Delta E)$, ○) plots and normalized electrochemical capacitance ($(\Delta Q/\Delta E)_n = -(W'/zF)$-$(\Delta Q/\Delta E)$, ●) plots ($W' = W_{Cs^+} = 132.9$), and (b, d, f) faradaic electrochemical capacitance ($\Delta Q^f/\Delta E^f$) plots at $E = -0.3$ V for PPy/PSS films (film thickness = (a, b) 1.5 μm, (c, d) 0.5 μm, and (e, f) 0.2 μm) in 0.5 M Cs_2SO_4.

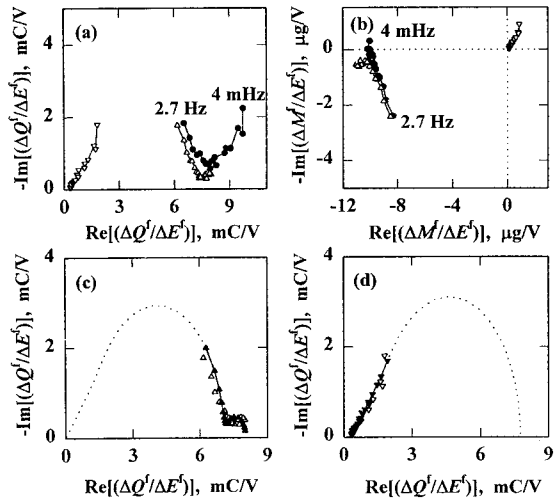

Figure 6. (a, c, d) Faradaic electrochemical capacitance ($\Delta Q^f/\Delta E^f$) plots and (b) faradaic electrogravimetric capacitance ($\Delta M^f/\Delta E^f$) plots at $E = -0.3$ V for PPy/PSS films (film thickness = 1.0 μm) in 0.5 M Cs_2SO_4 ($W_+' = W_{Cs^+} = 132.9$ and $W_-' = W_{SO_4^{2-}} = 96.0$); ($\Delta Q^f/\Delta E^f$) and ($\Delta M^f/\Delta E^f$) (●), ($\Delta Q^f{}_+/\Delta E^f$) and ($\Delta M^f{}_+/\Delta E^f$) (△), ($\Delta Q^f{}_-/\Delta E^f$) and ($\Delta M^f{}_-/\Delta E^f$) (▽), simulated ($\Delta Q^f{}_+/\Delta E^f$) (▲), and simulated ($\Delta Q^f{}_-/\Delta E^f$) (▼).

($\Delta Q^f/\Delta E^f$) plot consists of two semicircles. The semicircle in the higher frequency region relates to the fast charge transport process, whereas the semicircle in the lower frequency region relates to the slow charge transport process.[8] It seems that the ($\Delta M^f/\Delta E^f$) plot (Figure 6b) is the partial part of Figure 2a or Figure 2b, where the $R_{D+}C_{D+}$ time for a cation is smaller than the $R_{D-}C_{D-}$ time for an anion. The ($\Delta M^f/\Delta E^f$) data appear across the second and third quadrants. If ion transport was cation-specific, the ($\Delta M^f/\Delta E^f$) data would appear in the third quadrant only.[14a] It is evident that anion transport as well as

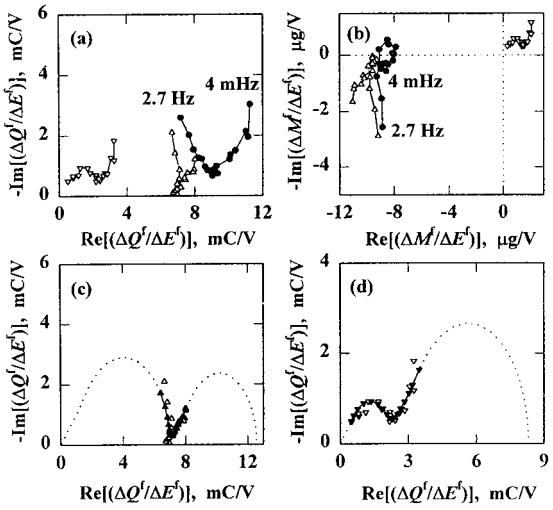

Figure 7. (a, c, d) Faradaic electrochemical capacitance ($\Delta Q^f/\Delta E^f$) plots and (b) faradaic electrogravimetric capacitance ($\Delta M^f/\Delta E^f$) plots at $E = -0.3$ V for PPy/PSS films (film thickness = 1.0 μm) in 1.0 M $CsNO_3$ ($W_+' = W_{Cs^+} = 132.9$ and $W_-' = W_{NO_3^-} = 62.0$); ($\Delta Q^f/\Delta E^f$) and ($\Delta M^f/\Delta E^f$) (●), ($\Delta Q^f{}_+/\Delta E^f$) and ($\Delta M^f{}_+/\Delta E^f$) (△), ($\Delta Q^f{}_-/\Delta E^f$) and ($\Delta M^f{}_-/\Delta E^f$) (▽), simulated ($\Delta Q^f{}_+/\Delta E^f$) (▲), and simulated ($\Delta Q^f{}_-/\Delta E^f$) (▼).

cation transport is considerable and that the diffusion coefficient of a cation is larger than that of an anion.

We showed that Y_{Cs^+} during the redox reaction of PPy/CuPTS films is negligible and that $Y_{SO_4^{2-}}$ during the redox reaction of PMPy/SO_4 films is less than 1.[14] However, because Y varies as the film/electrolyte system changes, it is difficult to know the exact Y_{Cs^+} and $Y_{SO_4^{2-}}$ in this system. Thus, the electrochemical capacitances of Cs^+ ($\Delta Q^f{}_+/\Delta E^f$) and SO_4^{2-} ($\Delta Q^f{}_-/\Delta E^f$) are obtained from ($\Delta Q^f/\Delta E^f$) and ($\Delta M^f/\Delta E^f$) by use of eqs 6 and 7 without consideration of water transport ($W_+' = W_{Cs^+}$ and $W_-' = W_{SO_4^{2-}}$). The ($\Delta Q^f{}_+/\Delta E^f$) and ($\Delta Q^f{}_-/\Delta E^f$) plots are shown in Figure 6a,c,d, and the ($\Delta M^f{}_+/\Delta E^f$) and ($\Delta M^f{}_-/\Delta E^f$) plots are shown in Figure 6b.

It is of interest to note that, in the same frequency range, the ($\Delta Q^f{}_-/\Delta E^f$) data appear at the left side of the semicircle whereas the ($\Delta Q^f{}_+/\Delta E^f$) data appear at the right side of the semicircle because R_DC_D time for Cs^+ is smaller than that for SO_4^{2-}. In Figure 6a, the frequency dependence of ($\Delta Q^f/\Delta E^f$) in the higher frequency region is similar to that of ($\Delta Q^f{}_+/\Delta E^f$), whereas the frequency dependence of ($\Delta Q^f/\Delta E^f$) in the lower frequency region is similar to that of ($\Delta Q^f{}_-/\Delta E^f$). This indicates that the semicircle of ($\Delta Q^f/\Delta E^f$) in the higher frequency region relates mainly to cation transport, whereas that in the lower frequency region relates mainly to anion transport. In Figure 6b, the ($\Delta M^f/\Delta E^f$) data appear in both the second and third quadrants, whereas the ($\Delta M^f{}_+/\Delta E^f$) data appear in the third quadrant and the ($\Delta M^f{}_-/\Delta E^f$) data appear in the first quadrant. If the data were extensively erroneous and the assumed W_+' and W_-' had large differences with the real ones, the ($\Delta M^f{}_+/\Delta E^f$) or ($\Delta M^f{}_-/\Delta E^f$) data would appear in more than two quadrants or in another quadrant.

A cyclic voltammogram and simultaneously acquired mass change diagram in a 1.0 M $CsNO_3$ solution are shown in Figure 3d. G_n is smaller than I in a wide potential range and is much smaller than G_n in a Cs_2SO_4 solution (Figure 3b). G_n for even the thick film in a $CsNO_3$ solution is smaller than I, while G_n in a Cs_2SO_4 solution is similar to I. It shows that NO_3^- transport in addition to Cs^+ transport is considerable. Figure 7a shows a ($\Delta Q^f/\Delta E^f$) plot and Figure 7b shows a ($\Delta M^f/\Delta E^f$) plot in a $CsNO_3$ solution. The ($\Delta Q^f/\Delta E^f$) plot is similar to that in a 0.5

TABLE 1: Values of the Parameters Obtained by Fitting the Electrochemical Capacitance Data Including Figure 6c,d and Figure 7c,d to the Equivalent Circuit of Figure 1c

			cation				anion			
solution	E, V	R_s, Ω	C_{D+1}, mF	$R_{D+1}C_{D+1}$, s	C_{D+2}, mF	$R_{D+2}C_{D+2}$, s	C_{D-1}, mF	$R_{D-1}C_{D-1}$, s	C_{D-2}, mF	$R_{D-2}C_{D-2}$, s
0.5 M Cs_2SO_4	−0.3	36	7.0	5.6×10^{-2}	1.1	17	0.32		7.5	410
0.5 M Cs_2SO_4	0.1	36	4.4	7.2×10^{-2}	0.39	3.8	0.58	8.7×10^{-2}	3.2	340
1.0 M $CsNO_3$	−0.3	29	6.9	4.7×10^{-2}	6.7	510	1.9	6.1×10^{-1}	6.4	340

M Cs_2SO_4 solution (Figure 6a), whereas the ($\Delta M^f/\Delta E^f$) plot is very complex. It was shown that $Y_{NO_3^-}$ during the redox reaction of PMPy/NO_3 and PPy/NO_3 films is small.[14b] Thus, the faradaic electrochemical capacitance of Cs^+ ($\Delta Q^f_+/\Delta E^f$) and the faradaic electrochemical capacitance of NO_3^- ($\Delta Q^f_-/\Delta E^f$) are obtained without consideration of water transport ($W_+' = W_{Cs^+}$ and $W_-' = W_{NO_3^-}$). It is interesting to note that both ($\Delta Q^f_+/\Delta E^f$) and ($\Delta Q^f_-/\Delta E^f$) plots consist of two semicircles. This means that cation transport occurs in both fast and slow charge transport processes and that anion transport also occurs in both fast and slow charge transport processes. In this case, the equivalent circuit in Figure 1c should be used instead of that in Figure 1b. The subscript 1 represents the ion transport in the fast charge transport process, and the subscript 2 represents the ion transport in the slow charge transport process.

In Figures 6 and 7, the ($\Delta Q^f_+/\Delta E^f$) data are fitted with parallel-connected $\boldsymbol{Z_{D+1}}$ and $\boldsymbol{Z_{D+2}}$, and also the ($\Delta Q^f_-/\Delta E^f$) data are fitted with parallel-connected $\boldsymbol{Z_{D-1}}$ and $\boldsymbol{Z_{D-2}}$. The values of fitted parameters are shown in Table 1. In a Cs_2SO_4 solution at both −0.3 and 0.1 V, anion transport is not large in the fast charge transport process and cation transport is not large in the slow charge transport. More detailed discussion is given in the Supporting Information. Consequently, it is evident that cation transport is dominant in the fast charge transport process, whereas anion transport is dominant in the slow charge transport process.

In a $CsNO_3$ solution, anion transport is considerable in the fast as well as slow charge transport process, and also cation transport is considerable in the slow as well as fast charge transport process (Table 1). It is interesting to note that C_{D+1} (=7.0 mF) at −0.3 V in a Cs_2SO_4 solution is similar to C_{D+1} (=6.9 mF) in a $CsNO_3$ solution. It shows that the amount of cation transport is constant irrespective of the presence of anion transport in the fast charge transport process. Thus, it is evident that the larger difference between G_n and I in a solution containing monovalent NO_3^- (Figure 3d) is due to the participation of considerable anion transport in the fast charge transport process. Thus, the ion transport behavior during the redox reaction of PPy/PSS films in a solution containing a monovalent anion is more complex than that in a solution containing a divalent anion.

It is shown that the discrepancy between the $(\Delta Q/\Delta E)_n$ plot and the ($\Delta M/\Delta E$) plot in Figure 5a,c,e increases as the film thickness decreases. Figure 5b,d,f shows the ($\Delta Q^f/\Delta E^f$) plots obtained from the ($\Delta Q/\Delta E$) plots of Figure 5a,c,e, respectively. In the frequency range from 2.72 Hz to 0.04 Hz, the ($\Delta Q^f/\Delta E^f$) data for the 1.5-μm film (Figure 5b) are located mostly in the semicircle of the fast charge transport process, whereas the ($\Delta Q^f/\Delta E^f$) data for the 0.2 μm film (Figure 5f) are located mostly in the semicircle of the slow charge transport process. And the ($\Delta Q^f/\Delta E^f$) data for the 0.5-μm film (Figure 5d) are located over two semicircles of the fast and slow charge transport processes. It is shown that, in this system, the fast charge transport process relates mainly to cation transport and the slow charge transport process relates mainly to anion transport. Thus, the $(\Delta Q/\Delta E)_n$ data (Figure 5a,c,e), obtained by assuming Cs^+-specific transport, have large difference with the ($\Delta M/\Delta E$) data in the frequency region where the slow charge transport process occurs. The discrepancy between the $(\Delta Q/\Delta E)_n$ and ($\Delta M/\Delta E$) data is larger in the thinner film because more data are located in the frequency region where the slow charge transport process occurs.

In the cyclic EQCM experiment (Figure 3a−c), it is shown that the influence of anion transport increases as the film thickness decreases. Considering the results in the impedance experiment, it seems that the fast charge transport process occurs mainly during the redox reaction of the 1.5-μm film, whereas the slow as well as fast charge transport process is considerable during the redox reaction of the 0.5- and 0.2-μm films. In the step EQCM experiment (Figure 4), it is shown that anion transport increases with time and that the relative contribution of an anion to ion transport is larger in the thinner film at the same measurement time. It seems that the fast charge transport process is dominant at the initial time, and then the slow charge transport process increases with time. The slow charge transport process becomes considerable in a short time as the film thickness decreases.

In the diffusion model,[2b,7d,8,16] the diffusion coefficient of an ion in a film (D) is calculated from the film thickness (l) and R_DC_D time as follows

$$D = l^2/R_DC_D \tag{8}$$

In the migration model,[17] D is given by

$$D = RT\sigma/F^2C_{IE} \tag{9}$$

where σ is the ionic conductivity in a film and C_{IE} is the concentration of ion-exchange sites in a film. Moreover,

$$\sigma = l/R_DA \tag{10}$$

$$C_{IE} \approx \int C_D dE/FAl \tag{11}$$

Therefore, D in the migration model is also approximately proportional to l^2/R_DC_D. When D is constant, R_DC_D time decreases with l. The frequency dependence of the semicircle in the ($\Delta Q/\Delta E$) plot relates to R_DC_D time. If R_DC_D time is smaller, the ($\Delta Q/\Delta E$) data in the same frequency range are located in the more right side of an electrochemical semicircle. Thus, if the frequency range is the same but the film thickness is different, the influence of the slow charge transport process is observed more in the thinner film. In the cyclic EQCM experiment, the two times decrement of l causes the same effect as the four times decrement of scan rate. And also, in the step EQCM experiment, the two times decrement of l causes the same effect as the four times decrement of measurement time. Thus, the influence of the slow charge transport process is observed more in the thinner film, if the scan rate for the thick film in the cyclic EQCM experiment or the measurement time in the step EQCM experiment is the same as that for the thin film.

Fast vs Slow Charge Transport Processes. It is shown that, in PPy/PSS films, cation transport is dominant in the fast charge

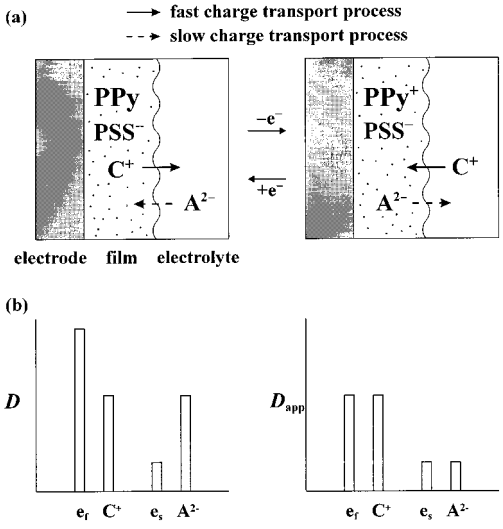

Figure 8. (a) Schematic diagrams of ion transport (A, anion; C, cation) and (b) the relative magnitude of the diffusion coefficient (D) and the apparent diffusion coefficient (D_{app}) in the fast and slow charge transport processes (e_f and e_s: electron in the fast and slow charge transport processes, respectively) during the redox reaction of PPy/PSS films in an aqueous solution containing a divalent anion.

transport process whereas anion transport is dominant in the slow one. Schematic diagrams of ion transport are shown in Figure 8a. Considering that charge transport in a film consists of electron transport and ion transport, there are two possible explanations for the presence of the slow charge transport process. One is that it is due to slow ion transport process. The other is that it is due to slow electron transport process.

Generally, the kinetics of charge transport in a conducting polymer film has been explained by the easiness/difficulty of ion transport,[4,18] because ion transport is much slower than electron transport.[19] It has been proposed that, in PPy films, the fast charge transport process is due to a shallowly trapped ion, whereas the slow charge transport process is due to a deeply trapped ion by modeling two kinds of ionic trapping sites in a film and assuming only one kind of ion transport.[8] Actually, this model cannot be applied in this system because the dominant ion in the fast charge transport process is different from that in the slow one. It is also probable that the fast charge transport process is due to the easy movement of a shallowly trapped ion whereas the slow charge transport process is due to counter ion movement because of the immobility of a deeply trapped ion.[20] Two kinds of ion transport are assumed in this model. But, in a $CsNO_3$ solution (Figure 7), both cation and anion transport occur in the slow as well as fast charge transport process. This model cannot be applied, too. Thus, the presence of the slow charge transport process cannot be explained by the easiness/difficulty of ion transport, or two kinds of ionic trapping site.

It has been shown that, in the electrochemical and electro-optical impedance[8,21] experiments for PPy films, the electro-optical capacitance plot at 780 nm wavelength consists of two semicircles, whereas the plot at 410 nm wavelength consists of only one semicircle, while the electrochemical capacitance plot consists of two semicircles.[22] From this result, it has been proposed that the fast charge transport process consists of two kinds of electron transport process, whereas the slow charge transport process consists of one kind of electron transport process. This means that electron transport process in the slow charge transport process is different from that in the fast charge transport process. When one kind of electron transport is present, only two kinds of ion transport are possible. In a $CsNO_3$ solution, there are four kinds of ion transport. If there were one kind of electron transport, it would be impossible. This also indicates that electron transport process in the slow charge transport process is different from that in the fast charge transport process.

In a Cs_2SO_4 solution (Table 1), $R_{D-2}C_{D-2}$ time is approximately 10^4 times larger than $R_{D+1}C_{D+1}$ time. This means that the apparent diffusion coefficient of SO_4^{2-} in the slow charge transport process is 10^4 times smaller than that of Cs^+ in the fast one. The difference between two apparent diffusion coefficients of a cation and an anion is very large. However, if the slow as well as fast charge transport process were governed by ion transport, the difference would be small. It seems that electron transport in the slow charge transport process is much slower than ion transport while ion transport in the fast charge transport process is much slower than electron transport. Thus, the small apparent diffusion coefficient of an ion in the slow charge transport process can be explained by slow electron transport, not slow ion transport. Consequently, the slow charge transport process is due to slow electron transport process, not slow ion transport process. It seems that the fast charge transport process is kinetically limited by ion transport whereas the slow charge transport process is by electron transport. More detailed discussion is given in the Supporting Information. Figure 8b shows the relative magnitude of the diffusion coefficient and the apparent diffusion coefficient in the fast and slow charge transport processes. The apparent diffusion coefficient in the fast charge transport process is related mainly to ion transport, whereas the apparent diffusion coefficient in the slow charge transport process is related mainly to electron transport.

Conclusions

We studied quantitatively the ion transport behavior in the slow as well as the fast charge transport process of PPy/PSS films. The slow charge transport process is due to slow electron transport process, not slow ion transport process. The fast charge transport process is kinetically limited by ion transport whereas the slow charge transport process is by electron transport. Anion transport is considerable in the slow charge transport process, while cation transport is dominant in the fast charge transport process. In the cyclic EQCM experiment, anion transport become considerable as the film thickness decreases. Moreover, in the step EQCM experiment, anion transport become considerable in a short time as the film thickness decreases. This results from the increase of the slow charge transport process.

Acknowledgment. This work was supported by the Korea Science and Engineering Foundation (Grant 94-0800-07-01-3).

Supporting Information Available: Details of capacitance data treatment and discussion (7 pages). See any current masthead page for ordering information and Web access instructions.

References and Notes

(1) (a) Evans, G. P. *Advances in Electrochemical Science and Engineering*; Gerischer, H., Tobias, C. W., Eds.; VCH: Weinheim, 1990; Vol. 1, p 1. (b) Heinze, J. *Synth. Met.* **1991**, *41*−*43*, 2805.

(2) (a) Inzelt, G. *Electroanalytical Chemistry*; Bard, A. J., Ed.; Marcel Dekker: New York, 1994; Vol. 18, p 89. (b) Lyons, M. E. G. *Electroactive Polymer Electrochemistry*; Lyons, M. E. G., Ed.; Plenum: New York, 1994; Part 1, p 1.

(3) Novák, P; Müller, K.; Santhanam, K. S. V.; Haas, O. *Chem. Rev.* **1997**, *97*, 207.

(4) (a) Maia, G.; Torresi, R. M.; Ticianelli, E. A.; Nart, F. C. *J. Phys. Chem.* **1996**, *100*, 15910. (b) John, R.; Wallace, G. G. *J. Electroanal. Chem.* **1993**, *354*, 145. (c) Bose, C. S. C.; Basak, S.; Rajeshwar, K. *J. Phys. Chem.* **1992**, *96*, 9899. (d) Naoi, K.; Lien, M.; Smyrl, W. H. *J. Electrochem. Soc.* **1991**, *138*, 440.

(5) (a) Buttry, D. A.; Ward, M. D. *Chem. Rev.* **1992**, *92*, 1355. (b) Buttry, D. A. *Electroanalytical Chemistry*; Bard, A. J., Ed.; Marcel Dekker: New York, 1991; Vol. 17, p 1.

(6) (a) Reynolds, J. R.; Pyo, M.; Qiu, Y.-J. *J. Electrochem. Soc.* **1994**, *141*, 35. (b) Baker, C. K.; Qiu, Y.-J.; Reynolds, J. R. *J. Phys. Chem.* **1991**, *95*, 4446.

(7) (a) Bruce, P. G. *Polymer Electrolyte Reviews-1*; MacCallum, J. R., Vincent, C. A., Eds.; Elsevier: London, 1987; Chapter 8. (b) Macdonald, J. R. *Impedance Spectroscopy*; Wiley: New York, 1987. (c) Musiani, M. M. *Electrochim. Acta* **1990**, *35*, 1665. (d) Albery, W. J.; Elliott, C. M.; Mount, A. R. *J. Electroanal. Chem.* **1990**, *288*, 15.

(8) Amemiya, T.; Hashimoto, K.; Fujishima, A. *J. Phys. Chem.* **1993**, *97*, 4187.

(9) (a) Amemiya, T.; Hashimoto, K.; Fujishima, A. *J. Phys. Chem.* **1993**, *97*, 9736. (b) Ren, X.; Pickup, P. G. *J. Phys. Chem.* **1993**, *97*, 3941. (c) Ren, X.; Pickup, P. G. *Electrochim. Acta* **1996**, *41*, 1877.

(10) (a) Sabatani, E.; Gafni, Y.; Rubinstein, I. *J. Phys. Chem.* **1995**, *99*, 12305. (b) Rubinstein, I.; Sabatani, E.; Rishpon, J. *J. Electrochem. Soc.* **1987**, *134*, 3078. (c) Glarum, S. H.; Marshall, J. H. *J. Electrochem. Soc.* **1987**, *134*, 142.

(11) Rishpon, J.; Gottesfeld, S. *J. Electrochem. Soc.* **1984**, *131*, 1960.

(12) (a) Bourkane, S.; Gabrielli, C.; Keddam, M. *Electrochim. Acta* **1989**, *34*, 1081. (b) Gabrielli, C.; Tribollet, B. *J. Electrochem. Soc.* **1994**, *141*, 1147.

(13) (a) Cordoba-Torresi, S.; Gabrielli, C.; Keddam, M.; Takenouti, H.; Torresi, R. *J. Electroanal. Chem.* **1990**, *290*, 269. (b) Gabrielli, C.; Keddam, M.; Perrot, H.; Torresi, R. *J. Electroanal. Chem.* **1994**, *378*, 85. (c) Bohnke, O.; Vuillemin, B.; Gabrielli, C.; Keddam, M.; Perrot, H. *Electrochim. Acta* **1995**, *40*, 2765.

(14) (a) Yang, H.; Kwak, J. *J. Phys. Chem. B* **1997**, *101*, 774. (b) Yang, H.; Kwak, J. *J. Phys. Chem. B* **1997**, *101*, 4656.

(15) Raistrick, I. D. *Electrochim. Acta* **1990**, *35*, 1579.

(16) (a) Penner, R. M.; Martin, C. R. *J. Phys. Chem.* **1989**, *93*, 984. (b) Panero, S.; Prosperi, P.; Passerini, S.; Scrosati, B.; Perlmutter, D. D. *J. Electrochem. Soc.* **1989**, *136*, 3729.

(17) (a) Pickup, P. G. *J. Chem. Soc., Faraday Trans.* **1990**, *86*, 3631. (b) Paulse, C. D.; Pickup, P. G. *J. Phys. Chem.* **1988**, *92*, 7002. (c) Burgmayer, P.; Murray, R. W. *J. Phys. Chem.* **1984**, *88*, 2515.

(18) (a) Pei, Q.; Inganäs, O. *J. Phys. Chem.* **1993**, *97*, 6034. (b) Tanguy, J.; Mermilliod, N.; Hoclet, M. *J. Electrochem. Soc.* **1987**, *134*, 795.

(19) Duffitt, G. L.; Pickup, P. G. *J. Chem. Soc., Faraday Trans.* **1992**, *88*, 1417.

(20) Fletcher, S. *J. Chem. Soc., Faraday Trans.* **1993**, *89*, 311.

(21) Kalaji, M.; Peter, L. M. *J. Chem. Soc., Faraday Trans.* **1991**, *87*, 853.

(22) Amemiya, T.; Hashimoto, K.; Fujishima, A. *J. Electroanal. Chem.* **1994**, *377*, 143.